Atmospheric
Chemistry
and Physics
Discussions

Open Access

Response of Global Surface Ozone Distribution to Northern Hemispheric Sea Surface Temperature Changes: Implication for Long-Range Transport

Kan Yi[1], Junfeng Liu[1], George Ban-Weiss[2], Jiachen Zhang[2], Wei Tao[1], Shu Tao[1]

[1] Laboratory for Earth Surface Processes, College of Urban and Environmental Sciences, Peking University, Beijing, China

[2] Sonny Astani Department of Civil and Environmental Engineering, University of Southern California, U.S.A.

Correspondence to: Junfeng Liu (E-mail: jfliu@pku.edu.cn)

Abstract

The response of surface O_3 concentrations to basin-scale warming and cooling of Northern Hemispheric oceans is investigated using the Community Earth System Model (CESM). Idealized spatially uniform sea surface temperature (SST) anomalies of +/- 1°C are superimposed onto the North Pacific, North Atlantic, and North Indian oceans, individually. Our simulations suggest seasonal and regional variability of surface O_3 in response to SST anomalies, especially in boreal summer. Increasing (decreasing) SST by 1 ℃ in one of the regions of focus induces decreases (increases) in surface O_3 concentrations, ranging from 1 to 5 ppbv. With fixed emissions, SST increases of a specific ocean in the Northern Hemisphere tend to increase summertime surface O_3 concentrations over upwind continents, accompanied with a widespread reduction over downwind regions. We implement the integrated process analysis (IPR) in CESM and find that meteorological O_3 transport in response to SST changes is the key process causing surface O_3 perturbations in most cases. During boreal summer, basin-scale SST warming facilitates vertical transport of O_3 to the surface over upwind

Atmospheric
Chemistry
and Physics
Discussions

Open Access

33 regions while significantly reducing vertical transport over continents that are

34 downwind. This process, as confirmed by tagged CO tracers, implicates a considerable

35 suppression of O_3 intercontinental transport due to increased stagnation at mid-latitudes

36 induced by SST increases. Changes in O_3 chemical production associated with regional

37 SST increases, on the other hand, can increase surface O_3 over highly polluted

38 continents except for South Asia. In South Asia, intensified cloud loading in response

39 to North Indian SST warming depresses both surface air temperature and solar radiation,

40 and thus photochemical production of O_3. Our findings indicate a robust linkage

41 between basin-scale SST variability and continental surface O_3 pollution, which should

42 be taken into account for regional air quality management.

43

44 **Keywords:** SST anomaly, Surface O_3, Process analysis, Transport, CESM

45

46

1. Introduction

48 Ground level ozone (O_3) adversely impacts human health (WHO., 2006) and threatens

49 food security (Chuwah et al., 2015). Considering its eco-toxicity, it is of great

50 importance to understand the physical and chemical mechanisms that control

51 atmospheric ozone concentrations. Surface O_3 is produced in the atmosphere via

52 photochemical processing of multiple precursors including volatile organic compounds

53 (VOCs), carbon monoxide (CO) and nitrogen oxides (NO, NO_2). These precursors

54 originate from both natural and anthropogenic sources (Vingarzan, 2004). In addition

55 to local production, transport of O_3 and its precursors from upwind regions and the

56 upper atmosphere can also influence surface O_3 abundance. Stratospheric intrusion

57 events, which lead to vertical down-mixing of ozone-rich air, can significantly elevate

58 surface O_3 during spring and summer (Lin et al., 2012;Zhang et al., 2014;Grewe, 2006).

59 Long-range transport of O_3 and its precursors have been extensively studied and their

60 inter-continental impacts have been evaluated with measurements and model

61 simulations (Fiore et al., 2009;Brown-Steiner and Hess, 2011).

Atmospheric
Chemistry
and Physics
Discussions

62

63   Both photochemistry and dynamic transport collectively affect surface O_3 levels.

64   Important meteorological factors that can impact both photochemistry and transport

65   include atmospheric circulations, solar radiation, and relative humidity. Atmospheric

66   circulations determine the timescale and pathway of O_3 transport (Auvray and Bey,

67   2005;Barnes and Fiore, 2013). Increases in solar radiation and air temperature can

68   increase the rate of chemical production of O_3, and modulate biogenic emissions of O_3

69   precursors (Sillman and Samson, 1995;Guenther, 1993;Peñuelas and Llusià, 2001),

70   especially over highly polluted regions (Ordónez et al., 2005;Pusede et al.,

71   2015;Rasmussen et al., 2012b). Increases in humidity can enhance the chemical

72   destruction of O_3 and shorten its atmospheric lifetime (Johnson et al., 1999;Camalier et

73   al., 2007). Therefore, changes in meteorological conditions at various spatial and

74   temporal scales play a key role in determining surface O_3 distribution. Understanding

75   the mechanisms and feedbacks of interactions between ozone and climate has received

76   increasing attention and will be essential for future surface ozone mitigation (Jacob and

77   Winner, 2009;Doherty et al., 2013).

78

79   Sea surface temperature (SST) is an indicator for both marine and terrestrial

80   meteorology. Its variations strongly perturb the mass and energy exchange between

81   ocean and atmosphere (Gulev et al., 2013;Small et al., 2008), which further influences

82   atmospheric circulation, solar radiation, atmospheric temperature and specific humidity

83   (Gill, 1982;Sutton and Hodson, 2005;Li et al., 2008;Frankignoul and Sennéchael, 2007)

84   from regional to global scales (Wang et al., 2000;Goswami et al., 2006;Glantz et al.,

85   1991). A number of studies have shown that SST changes over different oceans and

86   latitudes lead to significant different meteorological sensitivities and climate responses

87   (Lau, 1997;Webster, 1981;Sutton and Hodson, 2007;Lau and Nath, 1994). Details on

88   SST-climate relationships over individual oceanic regions are summarized in Kushnir

89   et al. (2002).

90

91   SSTs are generally increasing due to the impacts of anthropogenic global climate

Atmospheric
Chemistry
and Physics
Discussions

92   change (Pachauri et al., 2014). In addition, regional SST exhibits natural periodic or

93   irregular oscillations with timescales ranging from months to decades. The El

94   Niño/Southern Oscillation (ENSO) is the most influential natural SST variability

95   originating in the tropical Pacific with climate impacts worldwide (Philander,

96   1983;Wang et al., 2012). The Pacific decadal oscillation (PDO), defined by ocean

97   temperature anomalies in the northeast and tropical Pacific Ocean, is another long-lived

98   El Niño-like pattern persistent for several decades (Mantua and Hare, 2002). Over the

99   Indian Ocean, SST anomalies feature a seesaw structure between the western and

100 eastern equatorial regions, known as the Indian Ocean Dipole (IOD) mode (Saji et al.,

101 1999). The North Atlantic Ocean pronounces various modes of low-frequency SST

102 variability according to observations (Fan and Schneider, 2012;Wu and Liu,

103 2005;Kushnir, 1994;Taboada and Anadon, 2012). The mechanisms responsible for the

104 SST variability includes ocean circulation variability, wind stress， and ocean-

105 atmosphere feedbacks (Deser et al., 2010;Frankignoul, 1985). Emissions of aerosols

106 and greenhouse gases (GHGs) from anthropogenic and natural sources further

107 complicate regional SST variability because of their climate effects (Wu and Kinter,

108 2011;Hsieh et al., 2013;Rotstayn and Lohmann, 2002).

109

110 Considering the distinct roles of regional SST variability in modulating regional climate

111 system, there is a need to explore the impact of regional SST change on surface O_3

112 distribution. To date very few studies have been conducted to address the linkage

113 between SST- O_3 interactions except for the ENSO impacts-. For example,   Lin et al.

114 (2015) had found that more frequent deep stratospheric intrusions appear during ENSO

115 springs, which increase western US surface O_3 levels remarkably. However, a

116 comprehensive understanding of the response of surface O_3 to SST changes in

117 individual ocean basins is lacking.

118

119 To fill this gap, this study focuses on examining O_3 formation over four polluted

120 continental regions in the Northern Hemisphere (defined in Fiore et al. (2009)), and its

121 response to nearby basin-scale SST changes. We describe the design of numerical

Atmospheric
Chemistry
and Physics
Discussions

Open Access

EGU

122 experiments and model configuration in Section 2. Surface O_3 responses to regional

123 SST changes are given in Section 3. Relevant mechanisms governing the SST-O_3

124 relationships are discussed in Section 4. The impact of basin-scale SST changes on

125 inter-continental transport of O_3 is described in Section 5. Conclusions are drawn in

126 Section 6.

127 **2. Methodology**

128 **2.1 Model description and configuration**

129 The Community Earth System Model (CESM, v1.2.2) developed by the National

130 Center for Atmospheric Research (NCAR) is used in this study, configured with the

131 Community Atmosphere Model version 5.0 (CAM5) and the Community Land Model

132 version 4.0 (CLM4). The ocean and sea ice components are prescribed with

133 climatological SST and sea ice distributions. Moist turbulence is parameterized

134 following the Bretherton and Park (2009) scheme. Shallow convection is parameterized

135 using the Park and Bretherton (2009) scheme. The parameterization of deep convection

136 is based on Zhang and McFarlane (1995) with modifications following Richter and

137 Rasch (2008), Raymond and Blyth (1986), and Raymond and Blyth (1992). The cloud

138 microphysical parameterization is following a two-moment scheme described in

139 Morrison and Gettelman (2008) and Gettelman et al. (2008). The microphysical effect

140 of aerosols on clouds are simulated following Ghan et al. (2012). The parameterization

141 of cloud macrophysics follows Conley et al. (2012).

142

143 The chemistry coupled in the CAM5 (i.e., CAM5-chem) is primarily based on the

144 Model for O_3 and Related chemical Tracers, version 4 (MOZART-4), which resolves

145 85 gas-phase species, and 196 gas-phase reactions (Emmons et al., 2010;Lamarque et

146 al., 2012). A three-mode (i.e., Aitkin, accumulation and course) aerosol scheme for

147 black carbon (BC), primary organic matter (POM), second organic aerosol (SOA), sea

148 salt, dust and sulfate was used in our simulations following Liu and Ghan (2010). The

149 lightning parameterization is modified according to Price et al. (1997) and tropospheric

150 photolysis rates are calculated interactively following Tie et al. (2005). Gaseous dry

Atmospheric
Chemistry
and Physics
Discussions

Open Access

EGU

151   deposition is calculated using the resistance-based parameterization of Wesely (1989),

152   Walmsley and Wesely (1996), and Wesely and Hicks (2000). The parameterizations of

153   in-cloud scavenging and below-cloud washout for soluble species are described in

154   detail by Giorgi and Chameides (1985) and Brasseur et al. (1998), respectively.

155   Anthropogenic emissions of chemical species are from the IPCC AR5 emission datasets

156   (Lamarque et al., 2010), whose injection heights and particle size distributions follow

157   the AERCOM protocols (Dentener et al., 2006). The emissions of natural aerosols and

158   precursor gases are prescribed from the MOZART-2 (Horowitz et al., 2003) and

159   MOZART-4 (Emmons et al., 2010) datasets. All emission datasets are available from

160   the CESM data inventory (https://svn-ccsm-inputdata.cgd.ucar.Edu/trunk/inputdata/).

161   The performance of CESM in simulating tropospheric O_3 has been scientifically

162   validated by comparing with ozonesondes and satellite observations (Tilmes et al.,

163   2014). The deviations between model and observations are within the range of about

164   25%. In general, the model can capture the surface ozone distribution and variability

165   well, but may overestimate O_3 over the Eastern US and Western Europe in the summer

166   (Tilmes et al., 2014).

167

168   **2.2 Numerical Experiments**

169   We first conduct a control simulation, hereafter referred to as CTRL, with prescribed

170   climatological SSTs averaged from 1981 to 2010 (see Hurrell et al. (2008)). We then

171   conduct six perturbation simulations with monthly SSTs uniformly increased or

172   decreased by $1^{\circ}C$ in three ocean basins in the Northern Hemisphere: the North Pacific

173   (15°N-65°N;100°E-90°W), the North Atlantic Ocean (15°N-65°N; 100°W-20°E) and

174   the North Indian (5°N-30°N; 30°E-100°E). The simulations are denoted as "Pacific-

175   W", "Atlantic-W", "Indian-W" for three warming cases and "Pacific-C", "Atlantic-C",

176   "Indian-C" for three cooling cases. In each perturbation simulation, southern

177   boundaries of these oceanic regions are linearly smoothed to prevent large SST

178   gradients. Air pollution emissions, including biogenic emissions of VOCs, are held

179   fixed to distinguish the impacts of SST variation on O_3 transport and photochemistry.

180   All simulations are run for 12 years with the first year used for model spin-up.

Atmospheric
Chemistry
and Physics
Discussions

181

182 To explore the impacts of SST changes on inter-continental transport, an explicit

183 emission tagging technique is used in our simulations following previous studies

184 (Doherty et al., 2013;Shindell et al., 2008). Artificial CO-like tracers emitted from four

185 continental regions, i.e., North America (NA, 15°N–55 °N; 60°W–125°W), Europe

186 (EU, 25°N–65 °N; 10°W-50 °E), East Asia (EA, 15 °N–50 °N; 95°E–160 °E) and South

187 Asia (SA, 5 °N–35 °N; 50 °E–95°E), are tracked individually. These tracers are

188 idealized with a first-order decay lifetime of 50 days, which is similar to O_3 (Doherty

189 et al., 2013), and used to single out changes in O_3 transport induced by SST anomalies.

190

191 **2.3 Integrated process rate analysis**

192 To provide a process-level explanation on the response of surface O_3 to regional SST

193 changes, an integrated process rate (IPR) method is applied. This technique calculates

194 the accumulated contributions of individual processes to model predictions during

195 runtime, which has been widely used for air pollution diagnostics (Tao et al., 2015;Li

196 et al., 2012;Zhang and Wu, 2013). In this study, we add the IPR scheme to the CESM

197 modeling framework to track hourly contributions from 6 processes, including gas-

198 phase chemistry (CHEM), advection (ADVE), vertical diffusion (VDIF), dry

199 deposition (DRYD), shallow convection (SHAL) and deep convection (DEEP). The

200 wet deposition and aqueous phase chemistry are not considered here due to the

201 negligible solubility and production rate of O_3 in water (Jacob, 1999). The performance

202 of IPR is verified through comparing the predicted hourly O_3 changes with the sum of

203 individual burdens from the 6 processes during runtime. As shown in Figure S1, surface

204 O_3 abundance is well represented by the sum of these processes in the model.

205

206 **3. The response of surface O_3 concentrations to SST changes**

207 The responses of surface O_3 concentrations to basin-scale SST changes (i.e., $\pm 1°C$)

208 are investigated over four highly populated continental regions (Table 1). Seasonally

209 and regionally averaged surface O_3 changes (i.e., DJF (December, January, February),

Atmospheric
Chemistry
and Physics
Discussions

Open Access

EGU

210   MAM (March, April, May), JJA (June, July, August) and SON (September, October,

211   November)) for each SST perturbation simulation are mostly within 3 ppbv relative to

212   CTRL. Larger anomalies (i.e., up to 5ppbv) are simulated in locations including the east

213   coast of China, the Indian subcontinent, and remote oceans (Figure 1 and Figure S2).

214   This magnitude of O_3 change is comparable to intercontinental changes in ozone in

215   response to 20% reductions in anthropogenic emissions within a continental region

216   (Fiore et al., 2009).

217

218   As shown in Figure 1, up to 5 ppbv seasonal mean surface O_3 concentration changes

219   are found during boreal summers, mainly in coastal regions and remote oceans. Over

220   Southern China, increases in Northern Pacific SSTs lead to increases in surface O_3 of

221   nearly 3 ppbv, accompanied by decreases in North America (~1 ppbv, shown in Table

222   1).   In the "Atlantic-W" case, ground-level O_3 increases by nearly 1 ppbv over North

223   America, but decreases by 1~2 ppbv over Europe. Positive (negative) SST anomalies

224   in the Northern Indian Ocean lead to increases (decreases) in surface O_3 over the Indian

225   Ocean and Africa, but decreases (increases) over South and East Asia (Table 1).

226   Generally, we find that an increase (decrease) in summertime SST over a specific ocean

227   basin tends to increase (decrease) surface O_3 concentrations in upwind regions but

228   reduce (rise) that over downwind or remote continents. During boreal winters，a

229   widespread decrease (increase) of surface O_3 is observed associated with the warming

230   (cooling) of different oceans. Details are shown in Figure S2 in the supporting

231   information.

232

233   Our simulations reveal that changes in SSTs can impact region-specific complex

234   changes in surface O_3 distributions. We now focus on processes that impact the

235   dependency of SST on ozone distributions using the simulations that increase SST.

236   **4. Mechanism for SST induced surface O_3 changes.**

237   **4.1 Process-level response to SST changes**

238   Figure 2 shows the SST induced process-level changes spatially averaged over the four

Atmospheric
Chemistry
and Physics
Discussions

239   continental regions of interest (i.e., NA, EU, EA and SA). In most cases, vertical

240   diffusion (VDIF) and dry deposition (DRYD) are the key processes controlling the O_3

241   variation. Since both processes are closely dependent on the atmospheric turbulence

242   intensity, we define here a new term TURB as the sum of DRYF and VDIF, which can

243   represent the effect of turbulence intensity changes on surface O_3 variation. Meanwhile,

244   we also combine the shallow convection (SHAL) and deep convection (DEEP) as

245   CONV to represent the total convective contribution.

246

247   In the "Pacific-W" case, a SST anomaly of +1 ℃ over the North Pacific increases VDIF

248   in East Asia while significantly reducing it over North America. The corresponding

249   decrease of TURB in North America accounts for nearly 80 % of surface O_3 reduction

250   during JJA and SON while reductions of CONV are responsible for the remainder. In

251   the "Atlantic-W" run, similar increases in VDIF are simulated over North America.

252   However, it is accompanied by commensurate decreases in DRYD, resulting in an

253   insignificant overall change in TURB. The increase of CHEM therefore tends to

254   dominate the surface O_3 increase over North America. Relatively, TURB is more

255   important over Europe (JJA and SON only), leading to reduced surface O_3 abundances.

256   For "Indian-W", both CHEM and DEEP are reduced over South Asia in JJA and SON.

257   This reduction, though partially balanced by increases in ADVE and SHAL, leads to

258   overall reductions in surface O_3 over the Indian subcontinent (Figure 2).

259

260   The IPR analysis indicates that, in general, increases in SSTs in the North Pacific or

261   North Atlantic are more likely to elevate the vertical diffusion of O_3 over upwind

262   regions (i.e., East Asia and North America, respectively) but suppress it over remote

263   continents, especially in boreal summer. These opposite changes over upwind and

264   downwind regions lead to inconsistent surface O_3 responses. Changes in

265   photochemistry usually enhance surface O_3 formation except for South Asia where

266   advection and convection dominate the feedbacks of the Indian Ocean warming. In the

267   following subsections, the mechanisms responsible for the effects of SST changes in

268   different oceans on modulating relevant chemical and physical processes are further

Atmospheric
Chemistry
and Physics
Discussions

269   explored. We will focus on boreal summers since both surface O_3 levels and their

270   response to SST changes are highest during this period.

271

272   **4.2 Response of O_3 photochemical production to SST increase**

273   Figure 3 shows changes in net-production rate (i.e., chemical production rate minus loss

274   rate) of O_3 at the surface in JJA associated with basin-scale SST increases. Peak changes

275   are confined to the polluted regions owing to their high precursor emissions. For

276   example, an increase in North Pacific SSTs exerts a positive (negative) impact on net

277   O_3 production in the northern (southern) regions of East Asia. Similarly, the warming

278   of the North Atlantic promotes a dipole impact on the surface O_3 production over North

279   America, while the warming of North Indian Ocean significantly decreases the O_3 net-

280   production rate over South Asia.

281

282   As emissions are fixed in all simulations, the change in net O_3 production is driven by

283   SST induced meteorological changes (e.g., air temperature, air humidity, and solar

284   radiation). Figure 4 illustrates that an increase in SST of $1^\circ C$ in any ocean basin leads

285   to a widespread enhancement of surface air temperature (i.e., the air temperature at 2m)

286   over most continental areas. An exception is the North Indian Ocean, where an increase

287   in SST tends to cool the Indian subcontinent by $1-2^\circ C$. This temperature decrease is

288   not only limited to the surface, but also spreads to 600hPa (Figure S3). Associated with

289   this temperature decrease, there is a remarkable reduction of solar radiation received at

290   the continent beneath (more than 15 W/m^2, Figure S4). The SST increase over the North

291   Indian Ocean is believed to facilitate moist convection and cloud formation in the upper

292   troposphere, blocking solar radiation reaching the earth surface. This is consistent with

293   previous findings that moist convection is more sensitive to the SST changes in the

294   tropical oceans rather than mid- or high- latitude oceans (Lau et al., 1997;Lau and Nath,

295   1994).

296

297   A positive relationship between air temperature and O_3 chemical production has been

Atmospheric
Chemistry
and Physics
Discussions

298   well-documented previously (Jacob and Winner, 2009;Rasmussen et al., 2012a), and

299   thus the SST induced warming or cooling of air temperature is thought to be largely

300   responsible for the change in net O_3 production rate (Figure 3). On the other hand, the

301   SST increases also enhance evaporation of ocean water and increase humidity above

302   the respective ocean and its coastal areas (Figure S5), which may facilitate O_3

303   destruction and partially offset the positive influences of temperature changes. In

304   addition, over South Asia, warming of the North Indian Ocean decreases solar radiation

305   and air temperature, and simultaneously increases air humidity, which jointly destructs

306   O_3 production there.

307

308   **4.3 Response of O_3 physical transport to SST increase**

309   In Section 4.1, our IPR analysis highlights multiple important physical processes (i.e.,

310   vertical diffusion, convection and advection) on modulating surface O_3 concentrations.

311   However, the role and relative importance of each process exhibits large spatial

312   heterogeneity. In this section, we explore the key factors controlling O_3 physical

313   transport in response to basin-scale SST changes.

314

315   Figure 5 shows the surface pressure and wind pattern changes induced by a basin-wide

316   SST increase. Generally, a warming of any ocean basin will lead to a low-pressure

317   anomaly centered to its west at low-latitudes, which is caused by SST-induced

318   convective activity. As shown in Figure 6, the surface pressure reduction induced by

319   SST warming in any ocean basin is closely associated with enhanced upward motion

320   of air. Given that an SST threshold (about 26°−28°C) is required for deep convection

321   to generate, tropical oceans where meet this threshold are pronounced large-scale deep

322   convections and more sensitivity to SST anomalies (Johnson and Xie, 2010;Graham

323   and Barnett, 1987). Therefore, this low-pressure anomaly mainly occurs at low-

324   latitudes whereas the SST increase imposed at higher latitudes would have relatively

325   less effect on surface pressure changes (not shown here).

326

Atmospheric
Chemistry
and Physics
Discussions

327   Strengthened deep convection will trigger large-scale subsidence over adjacent regions,

328   which may suppress convective air movement over nearby continents (Lau et al., 1997).

329   This effect is confirmed by the widespread decreases of upward vertical velocity at 500

330   hPa depicted in Figure 6. Meanwhile, we also find that air temperature increase

331   associated with regional SST warming is more significant in the upper versus lower

332   troposphere, which leads to a decrease in the vertical air temperature gradient (shown

333   in Figure S3). These factors tend to enhance atmospheric stability and lead to a more

334   stagnant climate at mid-latitudes that restrains the vertical exchange of air pollutants.

335   The corresponding decrease in air ventilation contributes to the surface O_3

336   accumulation over polluted continental regions in JJA, but may weaken the intrusion

337   of O_3 from the upper troposphere to the surface in most clean regions. We believe this

338   effect to be responsible for the wide –spread decrease of surface O_3 associated in clean

339   regions with a SST increase as described in Section 3.

340

341   The surface pressure anomalies induced by SST changes can play a dominant role in

342   modulating surface O_3 transport at specific locations. For example, the low-pressure

343   anomaly centered over the east coast of Asia in the "Pacific-W" case tends to weaken

344   the East Asian summer monsoon (Figure 5a). Consequently, surface O_3 pollution is

345   enhanced in Southern China due to an increase of O_3 transport from the more polluted

346   Northern China (Figure 7a). Figure 7a also shows the vertical distribution of the

347   corresponding O_3 changes, zonally averaged over 100°E-130°E. It shows that the

348   increase of O_3 over Southern China is limited to below 700hPa, accompanied by a

349   noticeable decrease in the North and above. The IPR analysis indicates that the increase

350   in advective transport accounts for nearly 40% of the surface O_3 increase in the South

351   China, with the depressed turbulent/convective transport being responsible for the

352   remainder.

353

354   In the "Atlantic-W" run, the SST warming induced surface pressure anomalies lead to

355   substantial O_3 redistribution (Figure 7b). Ozone over North American is simulated to

356   have large changes in the upper troposphere and negligible changes at the surface.

Atmospheric
Chemistry
and Physics
Discussions

357 Therefore, as demonstrated in Section 4.1, the response of ground-level O_3 over North

358 America to the North Atlantic warming is mainly caused by enhanced photochemical

359 production, rather than physical transport.

360

361 As shown in Figure 5c, the North Indian SST warming leads to two surface pressure

362 anomalies, with one centered over the Arabian Sea and the other centered over the

363 Mediterranean. The warming of the North Indian Ocean strengthens the upward motion

364 of air at low-latitudes and further induces a convergence of highly polluted air over the

365 Indian Ocean. Effects of this process on O_3 concentrations are observed to be more

366 significant in the upper troposphere (Figure 7c). According to the IPR analysis, the

367 surface O_3 increase over the Indian Ocean is mainly caused by the downward diffusion

368 of O_3 from upper troposphere. However, over the nearby Indian subcontinent, the

369 suppressed deep convection accounts for nearly 20% of surface O_3 reduction there.

370

371 **5. Implication for O_3 long-range transport**

372 The above findings indicate that, in general, a basin-scale SST increase (decrease) in

373 the Northern Hemisphere is more likely to enhance (reduced) atmospheric stability at

374 mid-latitudes, which may suppress (promote) air pollutants from lofting to the free

375 troposphere. This potentially has large effects on O_3 intercontinental transport. We

376 follow previous work (e.g., (Doherty et al., 2013) and (Fang et al., 2011)) and use

377 passive CO-like tracers to demonstrate the potential effect of regional SST changes on

378 long-range O_3 transport. The surface changes of CO tracers originating from East Asia

379 in the "Pacific-W" run, North America in the "Atlantic-W" run, and South Asia in the

380 "Indian-W" run are displayed in Figure 8. A warming of North Pacific SSTs by 1°C

381 tends to increase the East Asian CO tracer concentrations by nearly 8% at the surface.

382 This is accompanied with a significant reduction (> 5%) of eastward transport to North

383 America (Figure 8a). Similarly, for the North American tracer, a warming of North

384 Atlantic SSTs by 1°C slightly increases (~2%) concentrations in North America but

385 decreases (3-4 %) concentrations over downwind Europe. These results suggest that the

Atmospheric
Chemistry
and Physics
Discussions

Open Access

386   warming (cooling) of SSTs tend to block (promote) trans-Pacific or trans-Atlantic

387   transport. The response of the Indian CO tracer to North Indian Ocean warming also

388   shows a decreasing tendency over downwind regions, but patterns are more

389   complicated over the source region in this case (Figure 8c).

390

391   The changes in upper tropospheric circulation generally shows that warming of SSTs

392   in different oceans tend to increase the 500-hPa geopotential height at mid-latitudes and

393   decrease it over polar areas (Figure 9). Additionally, the increase in North Indian SSTs

394   lead to geopotential height reductions above the Arabian Sea. The spatial pattern of

395   geopotential height anomalies at 500hPa is roughly consistent with that of air

396   temperature changes (Figure 9). This nonuniform increase in air temperature (i.e., more

397   significant at mid-latitudes) weakens the meridional temperature gradient, resulting in

398   a reduction of thermal winds. Therefore, the decreases in CO tracer transport to remote

399   regions can be well explained by both suppressed vertical ventilation and weakened

400   westerlies at mid-latitudes.

401

402   In addition, we also find a hemispheric-scale decrease of peroxyacetylnitrate (PAN), a

403   reservoir of O_3 precursors (NO_X and HO_X) that facilitates the long-range transport of

404   O_3, during the warming of different oceans (Figure S6). This decrease is likely to be

405   caused by the increase of the thermal decomposition of PAN responding to the air

406   temperature rise (Doherty et al., 2013;Jacob and Winner, 2009).

407

408   Thus, it is reasonable to infer in general that the increased thermal decomposition of

409   PAN, weakened mid-latitude westerlies, and reduced vertical ventilation may exert a

410   joint reducing effect on intercontinental transport of O_3 for basin-scale SST increases.

411

412   **6. Summary**

413   In this paper, we investigate the responses of surface O_3 to basin-scale SST anomalies

414   in the Northern Hemisphere. The latest version of CESM (version 1.2.2) is used in our

Atmospheric Chemistry and Physics
Open Access
Discussions
EGU

415   simulation forced with climatological and stationary SST anomalies ($\pm$ 1 ℃) in the

416   North Pacific, North Atlantic and North Indian Ocean, respectively. The responses of

417   surface O_3 associated with these SST changes are evaluated. Results of similar

418   magnitude but opposite sign are observed for the SST warming versus cooling

419   simulations for each ocean basin, suggesting robust connections between SST

420   anomalies and surface O_3 changes. The regionally and seasonally averaged surface O_3

421   changes over four continental regions (i.e., NA, EU, EA and SA) pronounce wide

422   seasonal and regional variability (varying from 1-3 ppbv). The warming of the North

423   Pacific leads to > 3 ppbv increases in surface O_3 over Southern China in summer, with

424   corresponding decreases over North America (~ 1 ppbv). Similarly, the North Atlantic

425   SST warming elevates surface O_3 pollution over North America while reducing surface

426   O_3 (nearly 1-2 ppbv) over Europe. Changes to North Indian SSTs exert significant

427   impacts (1-3ppbv) over South and East Asia during the entire year.

428

429   Process analysis indicates that dry deposition and vertical diffusion are two major

430   processes governing the surface ozone balance. The increase of SST in different ocean

431   basins tend to increase contributions of vertical diffusion to surface O_3 over upwind

432   regions while greatly restraining that over other remote continents. These processes

433   generally lead to a widespread decrease of surface O_3, which are partially offset by

434   increases in air temperature-dependent photochemical production rates. Specifically,

435   the photochemical production changes account for ~90% of surface O_3 increase over

436   North America in response to the North Atlantic SST warming, but exert a negative

437   effect on South Asia in response to the North Indian SST warming. Increases in

438   advective and convective transport of O_3 to the ground-level are significant over South

439   Asia associated with North Indian warming, which exerts an increasing influence on

440   surface O_3 concentrations. Advective transport also exerts an increasing influence on

441   surface O_3 in Southern China in the "Pacific-W" case.

442

443   We further reveal that air temperature is an important factor controlling surface O_3

444   responses to SST anomalies. Reductions in surface O_3 photochemical production in

Atmospheric
Chemistry
and Physics
Discussions

Open Access

EGU

445 Southern Asia associated with North Indian SST warming can be explained by the

446 corresponding SST-induced decreases in ground-level air temperature and solar

447 radiation. Meanwhile, the widespread increase of air temperature associated with basin-

448 scale SST warming is more likely to promote O_3 production over other highly polluted

449 regions.

450

451 On the other hand, SST increases over low latitudes of different oceans enhance deep

452 convection in the summer, which promotes convergence at the surface, as well as

453 upward ventilation in the low-latitudes. Corresponding surface pressure anomalies

454 centered over the east coast of Eastern Asia associated with the North Pacific warming

455 and over the Arabian Sea associated with the North Indian warming tend to increase

456 the surface O_3 above through exchanging with surrounding highly polluted air. The

457 basin-scale SST increases in the North Hemisphere promote a more stagnant climate

458 that restrains vertical transport of O_3 over continental regions as well as weakened mid-

459 latitude westerlies. The CO-tracer analysis suggests that these factors may have joint

460 negative effects on long-range transport of surface O_3.

461

462 Overall, our study highlights the sensitivity of the surface O_3 distribution to basin-wide

463 SST changes over different oceans in the Northern Hemisphere as well as the chemical

464 and dynamical factors that control it. We recommend that regional air quality

465 management of O_3 pollution should consider the influence of natural variability and

466 future increases in SSTs on ozone concentrations.

467

468 **Acknowledgements**

Atmospheric
Chemistry
and Physics
Discussions

Open Access

EGU

References:

474

475   Auvray, M., and Bey, I.: Long‐range transport to Europe: Seasonal variations and implications for the
476   European ozone budget, Journal of Geophysical Research: Atmospheres (1984 – 2012), 110, 2005.

477   Barnes, E. A., and Fiore, A. M.: Surface ozone variability and the jet position: Implications for projecting
478   future air quality, Geophys Res Lett, 40, 2839-2844, 10.1002/grl.50411, 2013.

479   Brasseur, G., Hauglustaine, D., Walters, S., Rasch, P., Müller, J. F., Granier, C., and Tie, X.: MOZART, a
480   global chemical transport model for ozone and related chemical tracers: 1. Model description,
481   Journal of Geophysical Research: Atmospheres, 103, 28265-28289, 1998.

482   Bretherton, C. S., and Park, S.: A new moist turbulence parameterization in the Community Atmosphere
483   Model, J Climate, 22, 3422-3448, 2009.

484   Brown-Steiner, B., and Hess, P.: Asian influence on surface ozone in the United States: A comparison of
485   chemistry, seasonality, and transport mechanisms, J Geophys Res-Atmos, 116, Artn
486   D1730910.1029/2011jd015846, 2011.

487   Camalier, L., Cox, W., and Dolwick, P.: The effects of meteorology on ozone in urban areas and their use
488   in assessing ozone trends, Atmos Environ, 41, 7127-7137, 2007.

489   Chuwah, C., van Noije, T., van Vuuren, D. P., Stehfest, E., and Hazeleger, W.: Global impacts of surface
490   ozone   changes   on   crop   yields   and   land   use,   Atmos   Environ,   106,   11-23,
491   10.1016/j.atmosenv.2015.01.062, 2015.

492   Conley, A. J., Garcia, R., Kinnison, D., Lamarque, J.-F., Marsh, D., Mills, M., Smith, A. K., Tilmes, S., Vitt, F.,
493   and Morrison, H.: Description of the NCAR community atmosphere model (CAM 5.0), NCAR
494   technical note, 2012.

495   Dentener, F., Kinne, S., Bond, T., Boucher, O., Cofala, J., Generoso, S., Ginoux, P., Gong, S., Hoelzemann,
496   J., and Ito, A.: Emissions of primary aerosol and precursor gases in the years 2000 and 1750
497   prescribed data-sets for AeroCom, Atmos Chem Phys, 6, 4321-4344, 2006.

498   Deser, C., Alexander, M. A., Xie, S.-P., and Phillips, A. S.: Sea surface temperature variability: Patterns
499   and mechanisms, Annual Review of Marine Science, 2, 115-143, 2010.

500   Doherty, R. M., Wild, O., Shindell, D. T., Zeng, G., MacKenzie, I. A., Collins, W. J., Fiore, A. M., Stevenson,
501   D. S., Dentener, F. J., Schultz, M. G., Hess, P., Derwent, R. G., and Keating, T. J.: Impacts of climate
502   change on surface ozone and intercontinental ozone pollution: A multi-model study, J Geophys
503   Res-Atmos, 118, 3744-3763, 10.1002/jgrd.50266, 2013.

504   Emmons, L., Walters, S., Hess, P., Lamarque, J.-F., Pfister, G., Fillmore, D., Granier, C., Guenther, A.,
505   Kinnison, D., and Laepple, T.: Description and evaluation of the Model for Ozone and Related
506   chemical Tracers, version 4 (MOZART-4), Geoscientific Model Development, 3, 43-67, 2010.

507   Fan, M., and Schneider, E. K.: Observed decadal North Atlantic tripole SST variability. Part I: weather
508   noise forcing and coupled response, J Atmos Sci, 69, 35-50, 2012.

509   Fang, Y., Fiore, A. M., Horowitz, L. W., Gnanadesikan, A., Held, I., Chen, G., Vecchi, G., and Levy, H.: The
510   impacts of changing transport and precipitation on pollutant distributions in a future climate,
511   Journal of Geophysical Research: Atmospheres, 116, 2011.

512   Fiore, A., Dentener, F., Wild, O., Cuvelier, C., Schultz, M., Hess, P., Textor, C., Schulz, M., Doherty, R., and
513   Horowitz, L.: Multimodel estimates of intercontinental source‐receptor relationships for ozone
514   pollution, Journal of Geophysical Research: Atmospheres (1984 – 2012), 114, 2009.

515   Frankignoul, C.: Sea surface temperature anomalies, planetary waves, and air‐sea feedback in the
516   middle latitudes, Reviews of geophysics, 23, 357-390, 1985.

Atmospheric
Chemistry
and Physics
Discussions

517 Frankignoul, C., and Sennéchael, N.: Observed influence of North Pacific SST anomalies on the
518   atmospheric circulation, J Climate, 20, 592-606, 2007.
519 Gettelman, A., Morrison, H., and Ghan, S. J.: A new two-moment bulk stratiform cloud microphysics
520   scheme in the Community Atmosphere Model, version 3 (CAM3). Part II: Single-column and global
521   results, J Climate, 21, 3660-3679, 2008.
522 Ghan, S. J., Liu, X., Easter, R. C., Zaveri, R., Rasch, P. J., Yoon, J.-H., and Eaton, B.: Toward a minimal
523   representation of aerosols in climate models: Comparative decomposition of aerosol direct,
524   semidirect, and indirect radiative forcing, J Climate, 25, 6461-6476, 2012.
525 Gill, A. E.: Atmosphere-ocean dynamics, Academic press, 1982.
526 Giorgi, F., and Chameides, W.: The rainout parameterization in a photochemical model, Journal of
527   Geophysical Research: Atmospheres, 90, 7872-7880, 1985.
528 Glantz, M. H., Katz, R. W., and Nicholls, N.: Teleconnections linking worldwide climate anomalies,
529   Cambridge University Press Cambridge, 1991.
530 Goswami, B., Madhusoodanan, M., Neema, C., and Sengupta, D.: A physical mechanism for North
531   Atlantic SST influence on the Indian summer monsoon, Geophys Res Lett, 33, 2006.
532 Graham, N., and Barnett, T.: Sea surface temperature, surface wind divergence, and convection over
533   tropical oceans, Science, 238, 657-659, 1987.
534 Grewe, V.: The origin of ozone, Atmos Chem Phys, 6, 1495-1511, 2006.
535 Guenther, R.: Isoprene and monoterpene emission rate variability: model evaluations and sensitivity
536   analyses, J Geophys Res, 98, 1993.
537 Gulev, S. K., Latif, M., Keenlyside, N., Park, W., and Koltermann, K. P.: North Atlantic Ocean control on
538   surface heat flux on multidecadal timescales, Nature, 499, 464-467, 2013.
539 Horowitz, L. W., Walters, S., Mauzerall, D. L., Emmons, L. K., Rasch, P. J., Granier, C., Tie, X., Lamarque, J.
540   F., Schultz, M. G., and Tyndall, G. S.: A global simulation of tropospheric ozone and related tracers:
541   Description and evaluation of MOZART, version 2, Journal of Geophysical Research: Atmospheres
542   (1984–2012), 108, 2003.
543 Hsieh, W. C., Collins, W. D., Liu, Y., Chiang, J. C. H., Shie, C. L., Caldeira, K., and Cao, L.: Climate response
544   due to carbonaceous aerosols and aerosol-induced SST effects in NCAR community atmospheric
545   model CAM3.5, Atmos Chem Phys, 13, 7489-7510, DOI 10.5194/acp-13-7489-2013, 2013.
546 Hurrell, J. W., Hack, J. J., Shea, D., Caron, J. M., and Rosinski, J.: A new sea surface temperature and sea
547   ice boundary dataset for the Community Atmosphere Model, J Climate, 21, 5145-5153, 2008.
548 Jacob, D.: Introduction to atmospheric chemistry, Princeton University Press, 1999.
549 Jacob, D. J., and Winner, D. A.: Effect of climate change on air quality, Atmos Environ, 43, 51-63, 2009.
550 Johnson, C., Collins, W., Stevenson, D., and Derwent, R.: Relative roles of climate and emissions changes
551   on future tropospheric oxidant concentrations, Journal of Geophysical Research: Atmospheres
552   (1984–2012), 104, 18631-18645, 1999.
553 Johnson, N. C., and Xie, S.-P.: Changes in the sea surface temperature threshold for tropical convection,
554   Nat Geosci, 3, 842-845, 2010.
555 Kushnir, Y.: Interdecadal variations in North Atlantic sea surface temperature and associated
556   atmospheric conditions, J Climate, 7, 141-157, 1994.
557 Kushnir, Y., Robinson, W., Bladé, I., Hall, N., Peng, S., and Sutton, R.: Atmospheric GCM response to
558   extratropical SST anomalies: Synthesis and evaluation*, J Climate, 15, 2233-2256, 2002.
559 Lamarque, J.-F., Bond, T. C., Eyring, V., Granier, C., Heil, A., Klimont, Z., Lee, D., Liousse, C., Mieville, A.,
560   and Owen, B.: Historical (1850–2000) gridded anthropogenic and biomass burning emissions of

Atmospheric
Chemistry
and Physics
Discussions

561   reactive gases and aerosols: methodology and application, Atmos Chem Phys, 10, 7017-7039,
562   2010.
563   Lamarque, J., Emmons, L., Hess, P., Kinnison, D. E., Tilmes, S., Vitt, F., Heald, C., Holland, E. A., Lauritzen,
564   P., and Neu, J.: CAM-chem: Description and evaluation of interactive atmospheric chemistry in
565   the Community Earth System Model, Geosci. Model Dev, 5, 369-411, 2012.
566   Lau, K., Wu, H., and Bony, S.: The role of large-scale atmospheric circulation in the relationship between
567   tropical convection and sea surface temperature, J Climate, 10, 381-392, 1997.
568   Lau, N.-C., and Nath, M. J.: A modeling study of the relative roles of tropical and extratropical SST
569   anomalies in the variability of the global atmosphere-ocean system, J Climate, 7, 1184-1207, 1994.
570   Lau, N.-C.: Interactions between global SST anomalies and the midlatitude atmospheric circulation, B
571   Am Meteorol Soc, 78, 21-33, 1997.
572   Li, L., Chen, C., Huang, C., Huang, H., Zhang, G., Wang, Y., Wang, H., Lou, S., Qiao, L., and Zhou, M.:
573   Process analysis of regional ozone formation over the Yangtze River Delta, China using the
574   Community Multi-scale Air Quality modeling system, Atmos Chem Phys, 12, 10971-10987, 2012.
575   Li, S., Lu, J., Huang, G., and Hu, K.: Tropical Indian Ocean basin warming and East Asian summer monsoon:
576   A multiple AGCM study, J Climate, 21, 6080-6088, 2008.
577   Lin, M., Fiore, A. M., Horowitz, L. W., Langford, A. O., Oltmans, S. J., Tarasick, D., and Rieder, H. E.: Climate
578   variability modulates western US ozone air quality in spring via deep stratospheric intrusions, Nat
579   Commun, 6, 2015.
580   Lin, M. Y., Fiore, A. M., Cooper, O. R., Horowitz, L. W., Langford, A. O., Levy, H., Johnson, B. J., Naik, V.,
581   Oltmans, S. J., and Senff, C. J.: Springtime high surface ozone events over the western United
582   States: Quantifying the role of stratospheric intrusions, J Geophys Res-Atmos, 117, Artn D00v22
583   10.1029/2012jd018151, 2012.
584   Liu, X., and Ghan, S.: A modal aerosol model implementation in the community atmosphere model,
585   version 5 (CAM5), J. Atmos. Sci, 2010.
586   Mantua, N. J., and Hare, S. R.: The Pacific decadal oscillation, J Oceanogr, 58, 35-44, 2002.
587   Morrison, H., and Gettelman, A.: A new two-moment bulk stratiform cloud microphysics scheme in the
588   Community Atmosphere Model, version 3 (CAM3). Part I: Description and numerical tests, J
589   Climate, 21, 3642-3659, 2008.
590   Ordónez, C., Mathis, H., Furger, M., Henne, S., Hüglin, C., Staehelin, J., and Prévôt, A.: Changes of daily
591   surface ozone maxima in Switzerland in all seasons from 1992 to 2002 and discussion of summer
592   2003, Atmos Chem Phys, 5, 1187-1203, 2005.
593   Pachauri, R. K., Allen, M., Barros, V., Broome, J., Cramer, W., Christ, R., Church, J., Clarke, L., Dahe, Q.,
594   and Dasgupta, P.: Climate Change 2014: Synthesis Report. Contribution of Working Groups I, II
595   and III to the Fifth Assessment Report of the Intergovernmental Panel on Climate Change, 2014.
596   Park, S., and Bretherton, C. S.: The University of Washington shallow convection and moist turbulence
597   schemes and their impact on climate simulations with the Community Atmosphere Model, J
598   Climate, 22, 3449-3469, 2009.
599   Peñuelas, J., and Llusià, J.: The complexity of factors driving volatile organic compound emissions by
600   plants, Biologia Plantarum, 44, 481-487, 2001.
601   Philander, S. G. H.: El Niño southern oscillation phenomena, Nature, 302, 295-301, 1983.
602   Price, C., Penner, J., and Prather, M.: NOx from lightning: 1. Global distribution based on lightning physics,
603   Journal of Geophysical Research: Atmospheres (1984–2012), 102, 5929-5941, 1997.
604   Pusede, S. E., Steiner, A. L., and Cohen, R. C.: Temperature and Recent Trends in the Chemistry of

Atmospheric
Chemistry
and Physics
Discussions

605   Continental Surface Ozone, Chem Rev, 115, 3898-3918, 10.1021/cr5006815, 2015.

606 Rasmussen, D., Fiore, A., Naik, V., Horowitz, L., McGinnis, S., and Schultz, M.: Surface ozone-temperature
607   relationships in the eastern US: A monthly climatology for evaluating chemistry-climate models,
608   Atmos Environ, 47, 142-153, 2012a.

609 Rasmussen, D. J., Fiore, A. M., Naik, V., Horowitz, L. W., McGinnis, S. J., and Schultz, M. G.: Surface ozone-
610   temperature relationships in the eastern US: A monthly climatology for evaluating chemistry-
611   climate models, Atmos Environ, 47, 142-153, 10.1016/j.atmosenv.2011.11.021, 2012b.

612 Raymond, D., and Blyth, A.: Extension of the stochastic mixing model to cumulonimbus clouds, J Atmos
613   Sci, 49, 1968-1983, 1992.

614 Raymond, D. J., and Blyth, A. M.: A stochastic mixing model for nonprecipitating cumulus clouds, J Atmos
615   Sci, 43, 2708-2718, 1986.

616 Richter, J. H., and Rasch, P. J.: Effects of convective momentum transport on the atmospheric circulation
617   in the Community Atmosphere Model, version 3, J Climate, 21, 1487-1499, 2008.

618 Rotstayn, L. D., and Lohmann, U.: Tropical rainfall trends and the indirect aerosol effect, J Climate, 15,
619   2103-2116, 2002.

620 Saji, N., Goswami, B., Vinayachandran, P., and Yamagata, T.: A dipole mode in the tropical Indian Ocean,
621   Nature, 401, 360-363, 1999.

622 Shindell, D., Chin, M., Dentener, F., Doherty, R., Faluvegi, G., Fiore, A. M., Hess, P., Koch, D., MacKenzie,
623   I., and Sanderson, M.: A multi-model assessment of pollution transport to the Arctic, Atmos Chem
624   Phys, 8, 5353-5372, 2008.

625 Sillman, S., and Samson, P. J.: Impact of temperature on oxidant photochemistry in urban, polluted rural
626   and remote environments, Journal of Geophysical Research: Atmospheres, 100, 11497-11508,
627   1995.

628 Small, R., Xie, S., O'Neill, L., Seo, H., Song, Q., Cornillon, P., Spall, M., and Minobe, S.: Air–sea interaction
629   over ocean fronts and eddies, Dynam Atmos Oceans, 45, 274-319, 2008.

630 Sutton, R. T., and Hodson, D. L.: Atlantic Ocean forcing of North American and European summer climate,
631   Science, 309, 115-118, 2005.

632 Sutton, R. T., and Hodson, D. L.: Climate response to basin-scale warming and cooling of the North
633   Atlantic Ocean, J Climate, 20, 891-907, 2007.

634 Taboada, F. G., and Anadon, R.: Patterns of change in sea surface temperature in the North Atlantic
635   during the last three decades: beyond mean trends, Climatic Change, 115, 419-431, 2012.

636 Tao, W., Liu, J., Ban-Weiss, G., Hauglustaine, D., Zhang, L., Zhang, Q., Cheng, Y., Yu, Y., and Tao, S.: Effects
637   of urban land expansion on the regional meteorology and air quality of eastern China, Atmos
638   Chem Phys, 15, 8597-8614, 2015.

639 Tie, X., Madronich, S., Walters, S., Edwards, D. P., Ginoux, P., Mahowald, N., Zhang, R., Lou, C., and
640   Brasseur, G.: Assessment of the global impact of aerosols on tropospheric oxidants, Journal of
641   Geophysical Research: Atmospheres, 110, 2005.

642 Tilmes, S., Lamarque, J.-F., Emmons, L., Kinnison, D., Ma, P.-L., Liu, X., Ghan, S., Bardeen, C., Arnold, S.,
643   and Deeter, M.: Description and evaluation of tropospheric chemistry and aerosols in the
644   Community Earth System Model (CESM1. 2), Geoscientific Model Development Discussions, 7,
645   8875-8940, 2014.

646 Vingarzan, R.: A review of surface ozone background levels and trends, Atmos Environ, 38, 3431-3442,
647   2004.

648 Walmsley, J. L., and Wesely, M. L.: Modification of coded parametrizations of surface resistances to

Atmospheric
Chemistry
and Physics

Discussions

649   gaseous dry deposition, Atmos Environ, 30, 1181-1188, 1996.

650   Wang, B., Wu, R., and Fu, X.: Pacific-East Asian teleconnection: how does ENSO affect East Asian climate?,
651   J Climate, 13, 1517-1536, 2000.

652   Wang, C., Deser, C., Yu, J.-Y., DiNezio, P., and Clement, A.: El Nino and southern oscillation (ENSO): a
653   review, Coral Reefs of the Eastern Pacific, 3-19, 2012.

654   Webster, P. J.: Mechanisms determining the atmospheric response to sea surface temperature
655   anomalies, J Atmos Sci, 38, 554-571, 1981.

656   Wesely, M.: Parameterization of surface resistances to gaseous dry deposition in regional-scale
657   numerical models, Atmospheric Environment (1967), 23, 1293-1304, 1989.

658   Wesely, M., and Hicks, B.: A review of the current status of knowledge on dry deposition, Atmos Environ,
659   34, 2261-2282, 2000.

660   WHO.: Air Quality Guidelines: Global Update 2005. Particulate Matter, Ozone, Nitrogen Dioxide and
661   Sulfur Dioxide, World Health Organization, 2006.

662   Wu, L., and Liu, Z.: North Atlantic Decadal Variability: Air-Sea Coupling, Oceanic Memory, and Potential
663   Northern Hemisphere Resonance*, J Climate, 18, 331-349, 2005.

664   Wu, R. G., and Kinter, J. L.: Shortwave radiation-SST relationship over the mid-latitude North Pacific
665   during boreal summer in climate models, Clim Dynam, 36, 2251-2264, DOI 10.1007/s00382-010-
666   0775-5, 2011.

667   Zhang, G. J., and McFarlane, N. A.: Sensitivity of climate simulations to the parameterization of cumulus
668   convection in the Canadian Climate Centre general circulation model, Atmos Ocean, 33, 407-446,
669   1995.

670   Zhang, L., Jacob, D. J., Yue, X., Downey, N. V., Wood, D. A., and Blewitt, D.: Sources contributing to
671   background surface ozone in the US Intermountain West, Atmos Chem Phys, 14, 5295-5309,
672   10.5194/acp-14-5295-2014, 2014.

673   Zhang, Y., and Wu, S.-Y.: Understanding of the Fate of Atmospheric Pollutants Using a Process Analysis
674   Tool in a 3-D Regional Air Quality Model at a Fine Grid Scale, Atmospheric and Climate Sciences,
675   3, 18, 2013.

676

677

678

679

680

681

682

683

684

685

686

687

Atmospheric
Chemistry
and Physics
Discussions

688 **Table 1.** Regionally and seasonally averaged (only land grid boxes are included)

689 changes in surface O_3 concentrations (ppbv) for basin-scale SST perturbation cases

690 relative to the control simulation. Positive (negative) changes which are significant at

691 the 0.1 level evaluated with a Student t-test are marked by red (blue).

Ozone (ppbv)			DJF	MAM	JJA	SON
North Pacific	+1° C	North America	-0.50**	-0.78**	-1.01**	-0.91**
		Europe	-0.50**	-0.71**	-0.23	-0.40
		East Asia	-0.96**	-0.92**	0.45	0.00
		South Asia	-1.37**	0.22	-0.63	0.58
	-1° C	North America	0.58**	0.38	0.58**	0.49**
		Europe	0.40*	0.35	-0.86**	0.41*
		East Asia	0.50*	0.18	-0.12	0.00
		South Asia	0.02	-1.22*	-0.05	-0.56
North Atlantic	+1° C	North America	-0.07	0.20	0.62**	0.46**
		Europe	0.37*	0.02	-1.77**	-0.83**
		East Asia	-0.50**	-0.61**	-0.26	-0.06
		South Asia	-0.41	-1.62**	-0.96**	-0.60*
	-1° C	North America	0.27	0.32	-0.35	-0.35*
		Europe	-0.33	0.24	0.52	-0.06
		East Asia	0.11	0.59**	0.64*	0.41
		South Asia	-0.08	-0.55	0.95*	0.21
North India	+1° C	North America	-0.40*	-0.31	-0.11	-0.08
		Europe	-0.30	0.29	-0.07	0.42
		East Asia	-0.67**	-0.63**	-0.57**	-1.56**
		South Asia	-1.30**	0.12	-2.06**	-2.33**
	-1° C	North America	-0.07	-0.10	0.31	-0.12
		Europe	-0.28	-0.09	-0.52	-0.27
		East Asia	0.22	0.69**	0.22	1.60**
		South Asia	-0.01	0.21	1.94**	1.70**

692 *significant at the 0.1 level from Student t-test using 11 years model result

693 **significant at the 0.05 level from Student t-test using 11 years model result

694
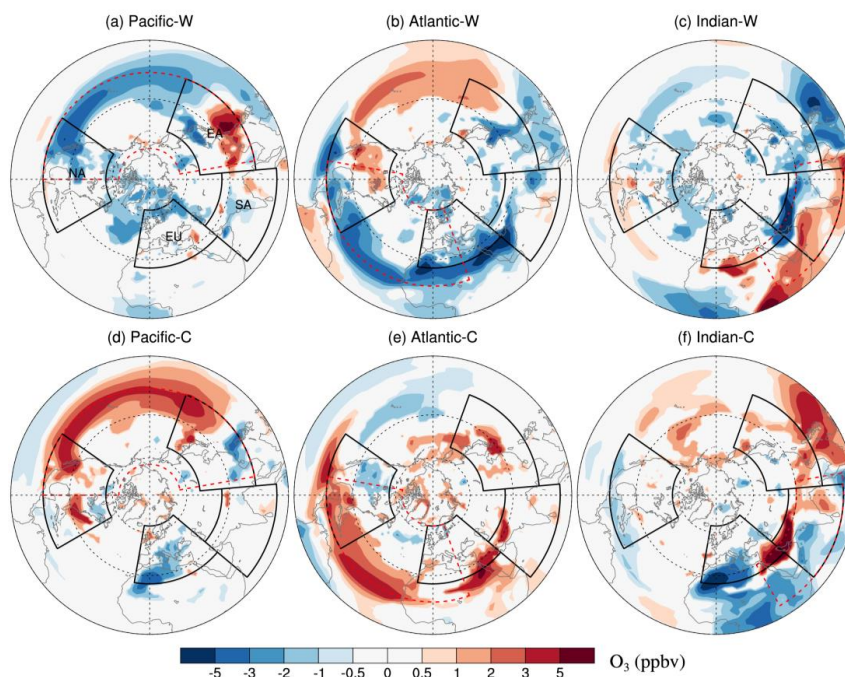
Figure 1. Changes in the summertime (June-August) surface ozone concentrations (ppbv) in the Northern Hemisphere induced by 1℃ warming (top) and 1℃ cooling (bottom) in the North Pacific Ocean (left), North Atlantic Ocean (center), and North Indian Ocean (right) relative to CTRL. Four major regions of interest (i.e., NA (15°N–55 °N; 60°W–125°W), EU (25°N–65 °N;10°W-50 °E), EA (15 °N–50 °N; 95°E–160 °E) and SA (5 °N–35 °N; 50 °E–95°E)) are marked with black polygons. Only results significant at the 0.1 level evaluated with a Student t-test using 11 years of data are depicted.

705
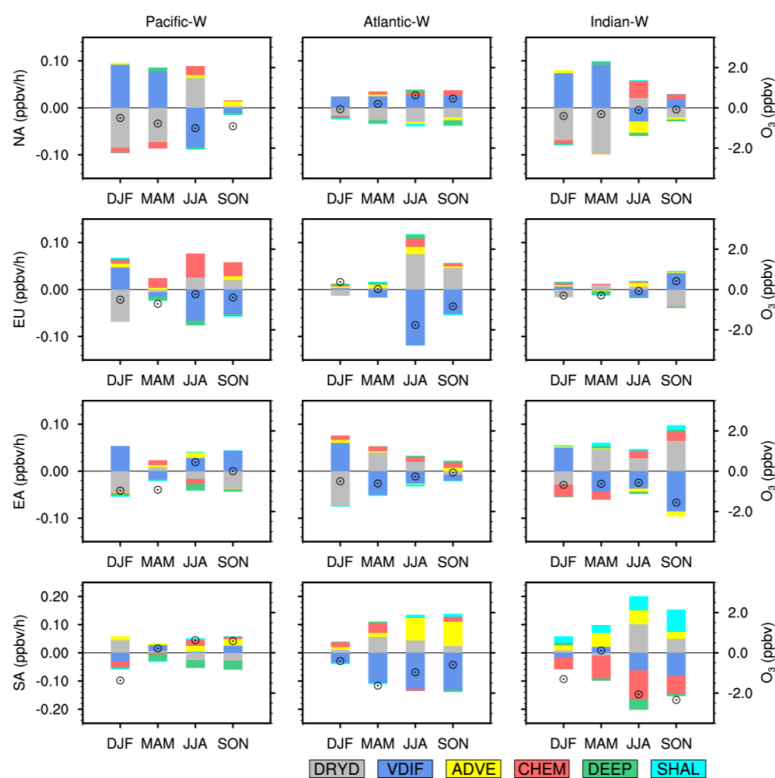
Figure 2. Seasonally averaged changes in IPR contributions (bars, ppbv/h, left scale)

707 and surface O_3 concentrations (hollow circles, ppbv, right scale) for Pacific-W (left),

708 Atlantic-W (middle) and Indian-W (right) relative to CTRL. Values are regionally

709 averaged over NA (first row), EU (second row), EA (third row) and SA (last row),

710 respectively. IPR contributions from six processes (i.e., gas-phase chemistry (CHEM),

711 advection (ADVE), vertical diffusion (VDIF), dry deposition (DRYD), shallow

712 convection (SHAL) and deep convection (DEEP)) are represented by different colors.

713

Atmospheric
Chemistry
and Physics
Discussions

Open Access

714
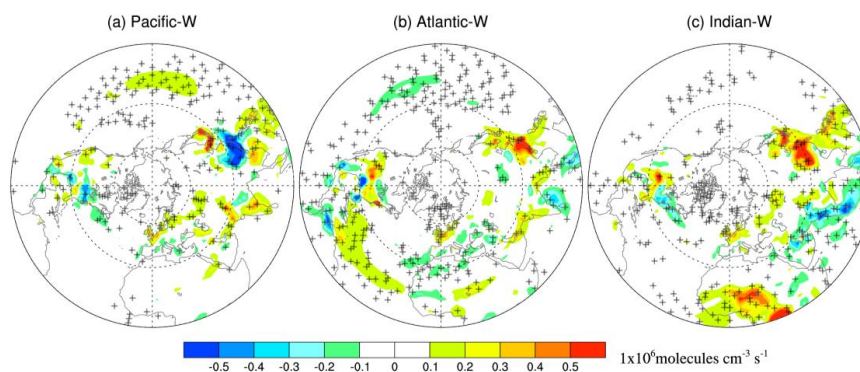
Figure 3. Perturbations of surface O_3 net-production rate (1×10^6 molecules cm^{-3} s^{-1})

relative to CTRL for (a) Pacific-W, (b) Atlantic-W, and (c) Indian-W in boreal summer.

The + symbols denote areas where results are significant at the 0.05 level as evaluated

with a Student t-test using 11 years of data.

719

720
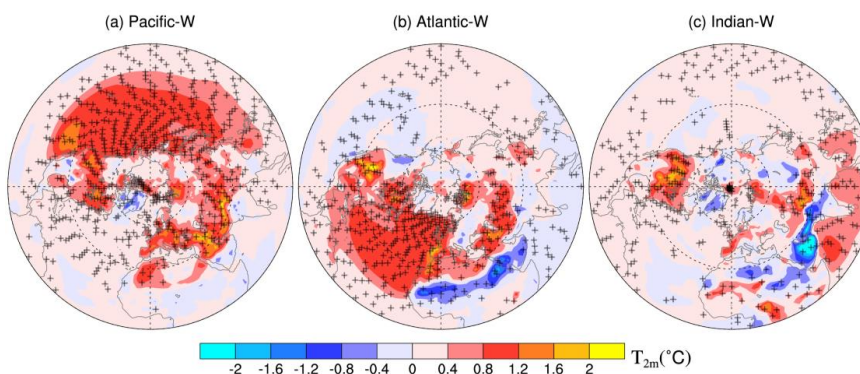
Figure 4.   The difference in surface air temperature (℃) for (a) Pacific-W, (b)

Atlantic-W, and (c) Indian-W relative to CTRL in the Northern Hemisphere in boreal

summer. The + symbols denote areas where results are significant at the 0.05 level as

evaluated with a Student t-test.

725

Atmospheric
Chemistry
and Physics
Discussions
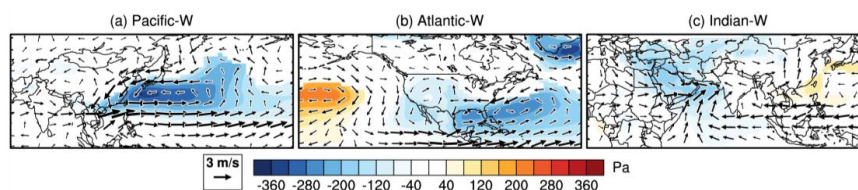
Figure 5. Changes in surface pressure (color contours, Pa) and wind pattern (arrows, m/s) for (a) Pacific-W, (b) Atlantic-W, and (c) Indian-W relative to CTRL in boreal summer. As for surface pressure changes, only results significant at the 0.05 level evaluated with a Student t-test are depicted.
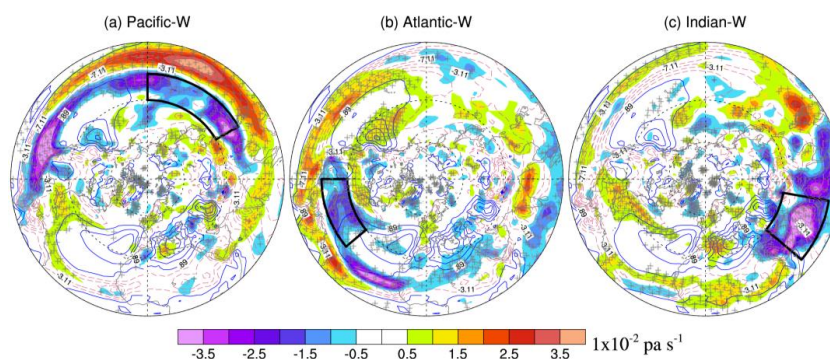

Figure 6. The spatial pattern of vertical velocity changes at 500 hPa (color contours, 1×10^{-2} Pa s^{-1}) for (a) Pacific-W, (b) Atlantic-W, and (c) Indian-W relative to CTRL. Contours with blue solid lines and red dashes indicate positive and negative downward vertical velocity in the control case, respectively (Contour interval: 2×10^{-2} Pa s^{-1}). Black polygons denote the regions where the surface pressure responses to SST anomalies are significant (see Figure 7 a-c). The + symbols indicate areas where results are significant at the 0.05 level as evaluated with a Student t-test using 11 years of data.

Atmospheric
Chemistry
and Physics
Discussions

Open Access
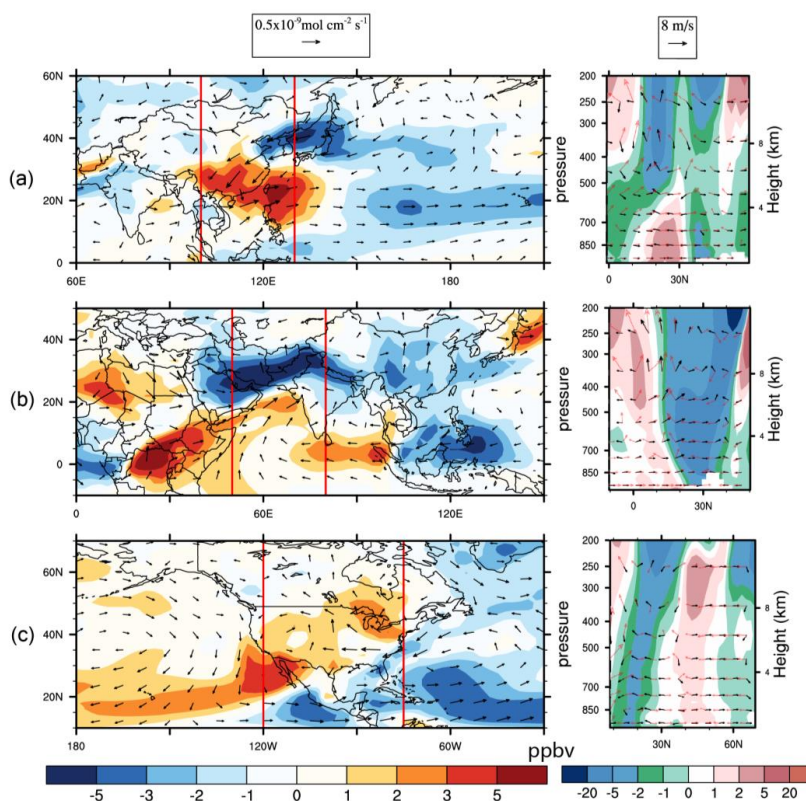
Figure 7. Left column: Changes in O_3 concentrations (color contours, ppbv) and horizontal fluxes (arrows, mol cm^{-2} s^{-1}) at surface level in boreal summer for (a) Pacific-W (top), (b) Atlantic-W (middle), (c) Indian-W (bottom) relative to CTRL. Right column: Longitude averaged vertical and latitudinal distributions of tropospheric O_3 changes (color contours, ppbv) and wind velocity in CTRL (red arrows, m/s) and its perturbation (black arrows, m/s) corresponding to the left. The red rectangles in the left column denote the longitudinal range used for average. The vertical velocity is amplified 1000 times to be comparable with horizontal velocity and distinct in the panels.

Atmospheric
Chemistry
and Physics
Discussions

755
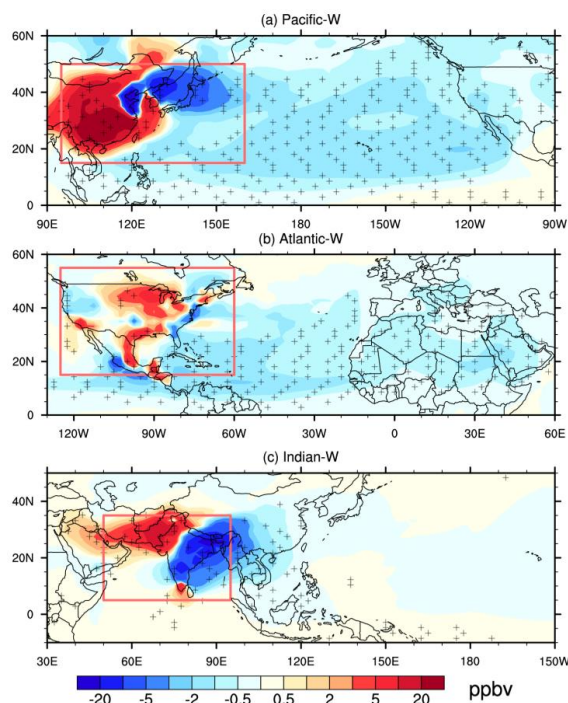
Figure 8.The difference in surface concentration (ppbv) of a CO-like tracer emitted in

(a) the East Asia for Pacific-W, (b) the North America for Atlantic-W and (c) the Indian

for Indian-W relative to CTRL. Red polygons denote the region where the CO-like

tracer emitted from. The + symbol denotes areas where the results are significant at the

0.05 level evaluated with a Student t-test.

761

762
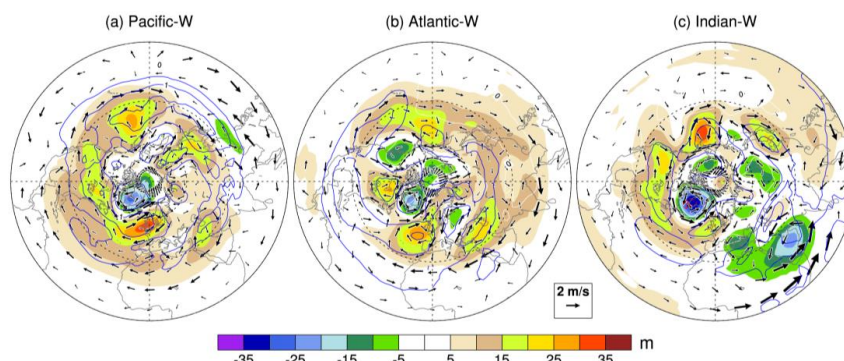
Figure 9. Changes in geopotential height (color contour, m), air temperature (contour,

$^{\circ}$C) and wind pattern anomalies (arrows, m s^{-1}) at 500hPa for (a) Pacific-W, (b)

Atmospheric
Chemistry
and Physics

Open Access

Discussions

EGU

765   Atlantic-W and (c) Indian-W relative to CTRL. Blue solid lines and red dashed lines in

766   the contours indicate positive and negative air temperature anomalies, respectively

767   (Contour interval: 0.5 °C).